Transitioning Plasma Actuators to Flight Applications

David Greenblatt, David Keisar and David Hasin

Abstract Pulse-modulated dielectric barrier discharge plasma actuators are applied to the problem of flow separation on a Hermes 450 unmanned air vehicle V-tail panel. Risk-reduction airfoil experiments were conducted followed by full-scale wind tunnel tests. Silicone-rubber based actuators were calibrated and subsequently retrofitted to both the airfoil and the panel. A lightweight (1 kg), flightworthy high-voltage generator was used to drive the actuators. Airfoil and full-scale panel wind tunnel experiments showed a mild sensitivity to actuation reduced frequencies and duty cycles. On the panel, actuation produced a significant effect on post-stall control authority: for $17° < \alpha < 22°$ a 100% increase in the post-stall lift coefficient was achieved; leading edge separation was prevented up to angles of attack of 30°; and hysteresis was virtually eliminated. Future research will focus on integrating the actuators into the panel geometry, implementing thicker dielectric materials and flight-testing.

Keywords Plasma · Actuators · Dielectric barrier discharge · Flight applications Unmanned air vehicle

D. Greenblatt (✉)
Faculty of Mechanical Engineering, Technion, Israel Institute of Technology, Haifa, Israel
e-mail: davidg@technion.ac.il
URL: https://www.flowcontrollab.com

D. Keisar
Grand Technion Energy Program, Technion, Israel Institute of Technology, Haifa, Israel

D. Hasin
Elbit Systems Ltd., Herzliya, Israel

© Springer Nature Switzerland AG 2019

R. King (ed.), *Active Flow and Combustion Control 2018*,
Notes on Numerical Fluid Mechanics and Multidisciplinary Design 141,
https://doi.org/10.1007/978-3-319-98177-2_7

1 Introduction

V-tail configurations are common on unmanned air vehicles (UAVs), but the tail panels suffer from flow separation, resulting in loss of control during crosswind take-off and landing [1, 2]. A potential solution to the problem is the application of plasma actuators at the leading-edges of the panels. Several studies have indicated that significant improvements to airfoil post-stall lift coefficients can be achieved, in some cases doubling the post-stall value [3–11]. Furthermore, leading-edge perturbations on vertical axis wind turbine blades dramatically increase turbine performance [12–15]. The actuators introduce perturbations corresponding to the separated shear layer instabilities. These perturbations grow and roll up into spanwise vortices that transport high-momentum flow to the panel surface [16]. This overcomes or ameliorates stall, exemplified by increases in maximum lift, significant increases in post-stall lift, elimination of hysteresis and drag reduction. In particular, single dielectric barrier discharge (SDBD, or simply DBD) plasma actuators are well-suited to typical takeoff and landing speeds [3].

Recently, DBD plasma actuators were demonstrated in-flight for the purpose of transition control [17]. A flightworthy system must fulfill a number of demanding requirements. Firstly, all components of the system must add insignificant mass to the payload and must require negligible power, as a fraction of propulsor power, for operation. The system must be operable on both sides of each control surface and normal operation should not compromise conventional flight control operation. If possible, initially, the system should not require complex feedback control and should be operable under open-loop or feedforward control. The system must be robust: namely, it must be operable for long periods without failure; if failure occurs, it must not compromise control of the vehicle relative to its original baseline configuration; and finally, the system must be easily manufactured, maintained, and repaired or replaced if necessary.

The global objective of this research is to implement DBD plasma actuators on the tail of a Hermes 450 unmanned air vehicle and conduct flight tests. This phase of the research has two main objectives: the first is to conduct wind tunnel experiments on a two-dimensional profile (airfoil) at takeoff speeds with different DBD plasma actuator configurations (risk-reduction experiments); the second is to conduct full-scale wind tunnel tests on a tail panel. The risk-reduction experiments are performed as a precursor to full-scale tests. A major challenge of this phase is to develop a flightworthy actuation system capable of producing sufficiently high-amplitude perturbations at typical takeoff and landing conditions. Here we consider a target takeoff speed of 43 kts or 22 m/s.

2 Airfoil Risk Reduction Experiments

2.1 Airfoil Design

An airfoil identical to the nominal panel section geometry, with a 350 mm chord length (c) and a 610 mm span (b), was designed and 3D printed (Fig. 1). The airfoil components comprise: (1) the main element; (2) the lower cover; (3) a removable leading-edge module; (4) a recessed removable leading-edge module. The main element is designed to carry the aerodynamic loads and removal of the lower cover facilitates access to the internal volume of the model. The recessed leading-edge module was designed for the purpose of integrating the DBD actuators into the airfoil geometry with minimum distortion of the original profile. The airfoil has 76 pressure ports (41 on the main body and 35 on the non-recessed leading-edge module) and these are close-coupled with two 32-port ESP pressure scanners (piezo-resistive transducers) mounted inside the model. The airfoil was installed and tested in the Technion's Unsteady Low-Speed Wind Tunnel (UWT) 610 mm × 1004 mm test section [18]. It embodies a pair of circular Plexiglas® windows which are held in place by aluminum rings (Fig. 2). The airfoil model was firmly connected to both windows and pitched about the quarter-chord position by rotating both rings synchronously via a servomotor and belt drives.

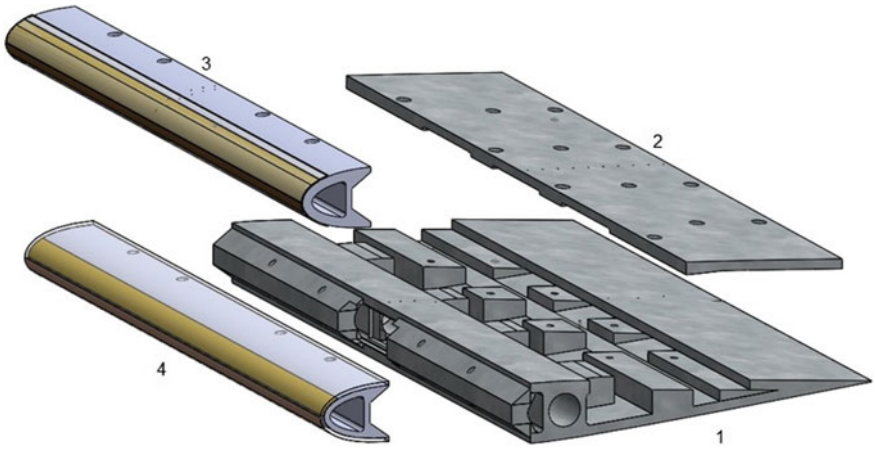

Fig. 1 Expanded schematic of the tail-panel airfoil for two-dimensional wind tunnel testing, showing: the main element (1); the lower cover (2); the removable leading edge modules [without recess (3), with recess (4)]

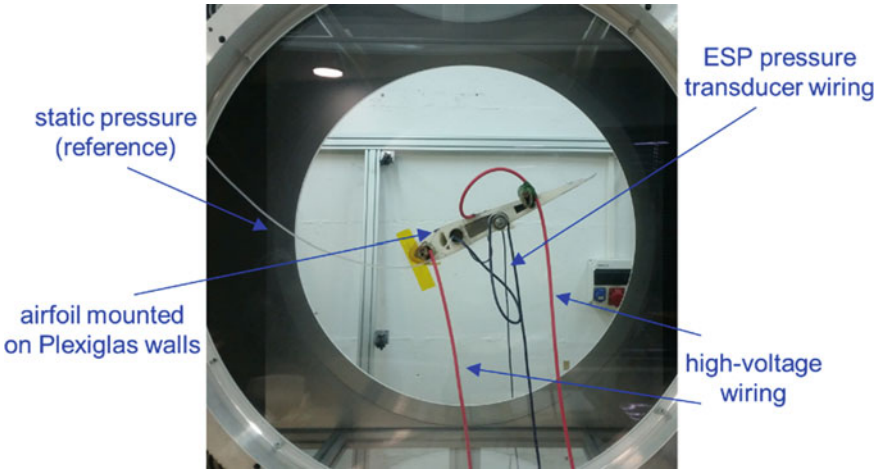

Fig. 2 Photograph of the airfoil with plasma actuator mounted in the tunnel. Pitch-down direction is defined as positive

2.2 DBD Plasma Actuators

In our previous wind turbine related research [12–15], DBD plasma actuators with upper (exposed) and lower (encapsulated) electrodes (both 70 μm thick) separated by three layers of 50 μm thick Kapton® tape were employed. These were wrapped around the leading-edge of the airfoils. For the present experiments, thicker silicone rubber dielectric material was employed (0.3–3 mm) that facilitated higher ionization voltages. Bench-top calibration experiments were performed for both the Kapton and silicone rubber dielectrics, where actuator thrust per unit length $|\mathbf{F}_b|$ was estimated using a Vibra AJ-200E balance. The actuators were driven by a modified GBS Elektronik Minipuls 2 high-voltage generator, consisting of an externally controllable transistor half-bridge and a high voltage transformer cascade. The generator was chosen principally for its low mass, namely 1.0 kg, which is a small fraction of the vehicle payload (150 kg). It requires an input signal and up to 40 V DC input voltage, that was supplied by either a CPx400D-Dual 420 watt DC laboratory power supply or a stack of lithium-ion polymer (LiPo) batteries.

For all calibrations, the ionization frequencies were in the range $8\,\text{kHz} \leq f_{\text{ion}} \leq 20\,\text{kHz}$; in the separation control study described below this signal was pulse-modulated at frequencies f_p. The power input was calculated from the measured DC voltage and the current supplied to the system: $\Pi_{\text{in}} = V_{\text{in}} \cdot I_{\text{in}}$. A summary of results is presented in Fig. 3, where the input power is referenced to the actuator length b_a.

Based on previous data [12–15], effective separation control was achieved at turbine blade relative wind speeds of 12 m/s. With a target free-stream velocity of 22 m/s, using dimensional analysis, it can easily be seen that the target actuator thrust

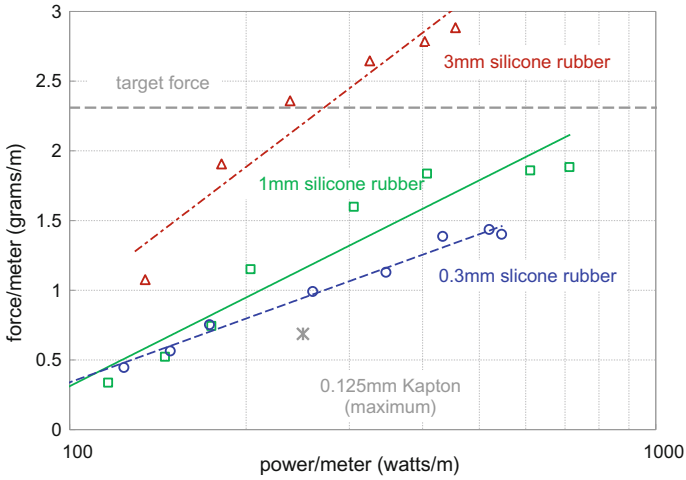

Fig. 3 Measured DBD plasma actuator thrust developed, at d.c. = 100%, as a function of measured input power to the high-voltage generator

must be $(22/12)^2 \cdot |\mathbf{F}_b|_{\text{Kapton}}$. Using silicone rubber as a dielectric material, the target force required for effective separation control at $U_\infty = 22$ m/s, corresponding to mid-span $Re = 7 \times 10^5$, can easily be obtained with a 3 mm thickness. However, in order to minimize changes to the nominal panel geometry, all experiments were performed with thickness 1 mm.

2.3 Airfoil Results

Preliminary baseline experiments at free-stream velocities $U_\infty = 19$ m/s and 29 m/s (corresponding to $Re = 4.3 \times 10^5$ and $Re = 6.5 \times 10^5$) were conducted without the actuator present, revealing excellent correspondence with the well-known prediction methods. Static stall occurred at 16° with a $C_{l,\max}$ of 1.3. After validating the fidelity of the baseline experimental setup, different experiments were conducted for the investigation of separation control at different Reynolds numbers, angles of attack, actuator configurations and power input. These were designated as risk-reduction experiments, conducted prior to the full-scale experiments described in Sect. 3. All experiments were performed with the actuator wrapped around the leading-edge of the airfoil, with the encapsulated and exposed electrodes in-line at the $x/c = 0$ location. Both 0.5 and 1.0 mm thick silicone rubber actuator dielectrics were evaluated.

Two key parameters employed for characterizing separation control studies [16] are the momentum coefficient, defined here as:

$$C_\mu \equiv b_a |\mathbf{F}_b| / (q_\infty S) \tag{1}$$

and

$$F^+ \equiv f_p c / U_\infty \tag{2}$$

where b_a, q_∞ and S are the actuator length, free-stream dynamic pressure and planform area respectively. For actuator calibrations $b_a \approx 20\,\text{cm}$, while for the airfoil and panel experiments b_a was equal to the span length. Typical values for effective leading-edge separation control are $C_\mu = \text{O}(0.1)\%$ and $F^+ = \text{O}(1)$. When the actuators are pulse-modulated, we can also define the net momentum flux that is directly proportional to the duty cycle, namely:

$$\langle C_\mu \rangle \equiv \text{d.c.} \times C_\mu \tag{3}$$

When the plasma ionization frequency is pulse-modulated, d.c. represents the fraction of the modulation period that the plasma is activated. From an applications point of view this is important because d.c. can be reduced to approximately 1%, without loss of airfoil or wing performance, but with a significant reduction in input power.

Since the actuator blocked most of the airfoil leading-edge surface, and the pressure ports with it, it was not possible to compare C_l changes with and without the plasma actuation (see Fig. 4). Therefore, to assess the *relative* changes in performance, three metrics were evaluated, namely: (i) $\Delta C_{p,\text{min}}$—the change in the minimum pressure coefficient; (ii) $\Delta C_{p,\text{TE}}$—the change in the pressure coefficient at the trailing edge of the airfoil; and (iii) $\Delta C_{l,\text{press}}$—the change in the lift coefficient contribution on the high pressure surface of the airfoil. The changes in the high-pressure surface of the airfoil are sensitive to overall circulation (or lift) and elimination of the ports near the leading-edge has only a small effect on the changes.

A summary of the three metrics is shown in Fig. 5 for the post-stall angle $\alpha = 24°$ employing a 0.5 mm thick dielectric. The changes in minimum pressure and lower surface pressure show similar dependence on reduced frequency, while the trailing-edge recovery shows a greater frequency sensitivity. However, the peak is not sharp and it can be concluded that a range of frequencies around $0.75 \leq F^+ \leq 1.5$ will produce positive and comparable increases to post-stall C_l. This is consistent with a number of other studies [16] and is a welcome result, in particular because for a given pulsation frequency, the full-scale panel F^+ varies as a function of the local chord-length (see Sect. 3). To illustrate this, Fig. 5 also shows the reduced frequency range, between root and tip, that would be encountered on the full-scale panel assuming $F^+ = 1$ at the mid-span. On the basis of this observation we project that the panel span-dependent modulation frequency, described in Sect. 3, will produce a positive beneficial result.

Figure 6 shows the variation of all metrics as a function of duty cycle (d.c.) and indicates similar effects for values between 1 and 10%. Duty cycle is a parameter of fundamental importance because the fraction of plasma activation determines the power input to the system [4]. Thus pulse-modulation at low duty cycles has a dual benefit because it can be configured to excite the most effective instability frequency at very low input power. These data are consistent with lift coefficient data acquired at

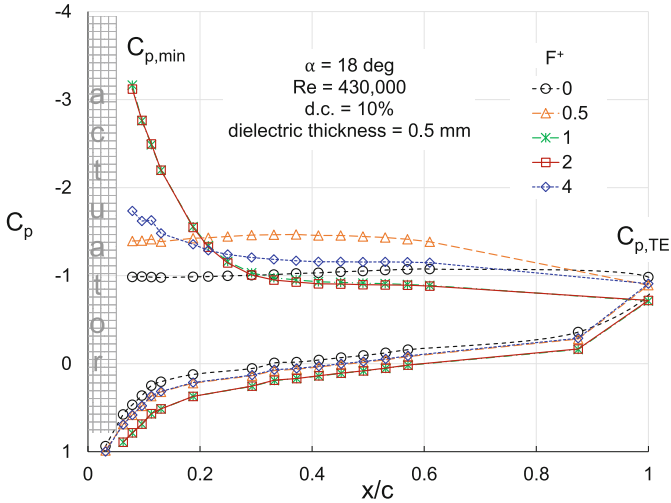

Fig. 4 Pressure coefficient distribution on the airfoil for different reduced frequencies. Actuation conditions: 0.5 mm thick silicone rubber, d.c. = 10%, $f_{\text{ion}} = 9,300$ Hz, $\Pi_{\text{in}} = 14$ W/m

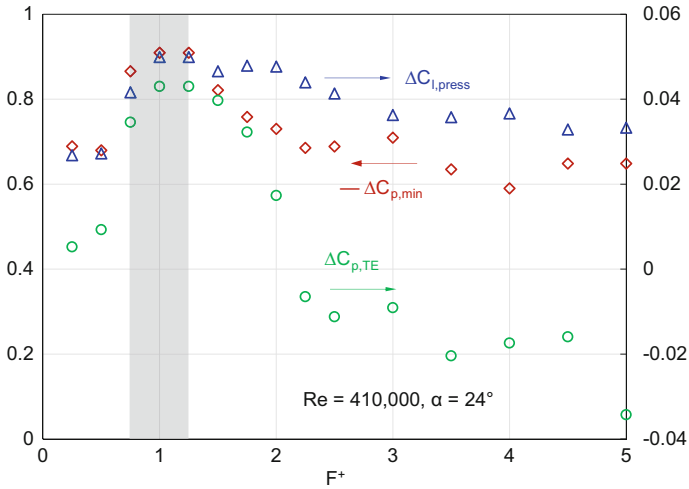

Fig. 5 $\Delta C_{p,\text{min}}$, $\Delta C_{p,\text{TE}}$ and $\Delta C_{l,\text{press}}$, for $0 \leq F^+ \leq 5$. Actuation conditions: 0.5 mm thick silicone rubber, d.c. = 10%, $f_{\text{ion}} = 9,300$ Hz, $\Pi_{\text{in}} = 14$ W/m. The shaded area indicates the F^+ range corresponding to the panel

lower Reynolds numbers, where a reduction of the duty cycle from 50 to 1% showed a lift insensitivity similar to [9, 11]. No attempt was made to reduce the d.c. further, although it should be noted that the lower limit should not be reduced to less than one full cycle, namely, d.c. $\geq f_p/f_{\text{ion}}$.

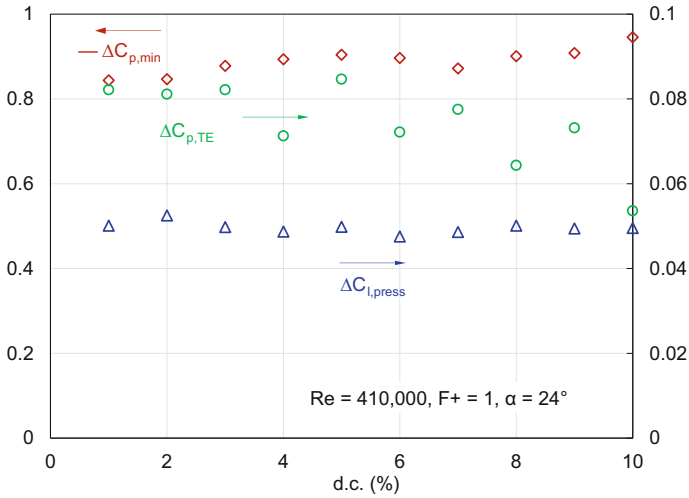

Fig. 6 Variation of the metrics $\Delta C_{p,\min}$, $\Delta C_{p,\mathrm{TE}}$ and $\Delta C_{l,\mathrm{press}}$ as a function of duty cycle, with $F^{+} = 1$

Finally, it was noted that the 1.0 mm thick silicone rubber-based actuator produced slightly superior results to those presented above. Moreover, no "burn-through" of the actuator was encountered during any of the experiments. Thus all experiments performed on the full-scale panel employed the 1.0 mm thick actuator.

3 Preliminary Tail-Panel Experiments

3.1 Experimental Setup

The Hermes 450 tail panel has a span of 1.6 m, root and tip chord lengths of 0.6 m and 0.35 m respectively, and a surface area of 0.747 m^2. Experiments were performed in Israel Aircraft Industry's (IAI's) closed-return low speed atmospheric wind tunnel, with test section dimensions 2.6 m × 3.6 m. The panel was mounted on a ∅1.2 m circular end-plate, and fastened to a six-component external aerodynamic balance by means of a clamp and flange (see Fig. 7). The balance operates on the multi-beam principle, employing stepper-motors to drive the riders along the beams to the null setting under each loading condition. The actuator was wrapped around the leading-edge of the panel and attached using double-sided tape in an identical manner to the airfoil application. For purposes of flow visualization, 28 mm fluorescent tufts were fixed to the panel, with 40 mm spacing between them. In order to achieve a strong contrast, the tail panel was painted matt-black and viewed under ultraviolet illumination. Smoke-base flow visualization was also performed.

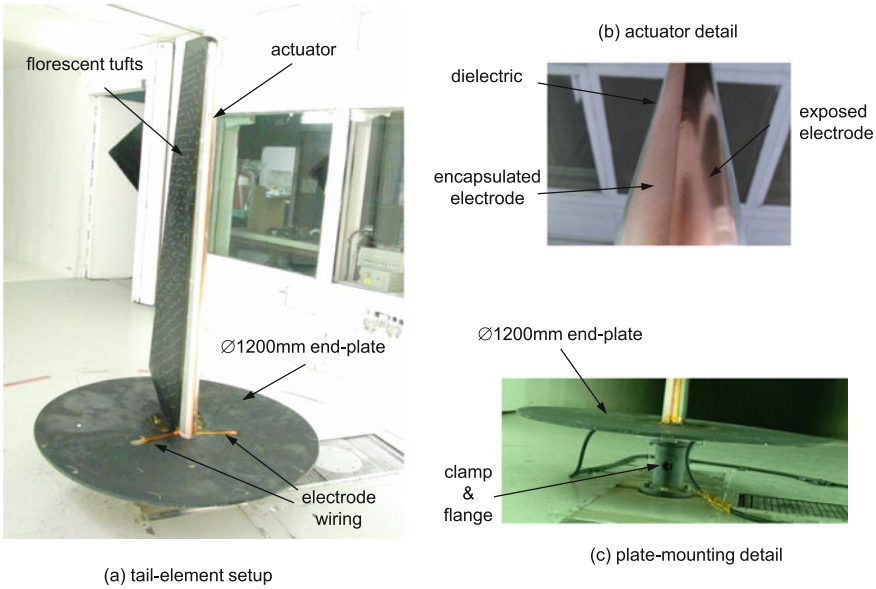

Fig. 7 Photographs of the full-scale panel experimental setup showing the assembly, actuator detail and mounting

3.2 Preliminary Results and Discussion

When pulsed perturbations are introduced, the reduced frequency is not uniquely defined because the chord-length is a function of the spanwise location. Here, we simply use the mean panel chord-length (475 mm) in the definition of F^+. Similar to the airfoil experiments, the panel was set at three post-stall angles of attack and for each angle, the pulsation frequency was swept corresponding to $0.25 \leq F^+ \leq 2.5$ at d.c. $= 10\%$ and $\Pi_{\text{gross}} = 8.7$ W. As before, experiments were performed by measuring the baseline value, followed by initiation of the pulsations, and a subsequent baseline measurement. These data are summarized in Fig. 8. The greatest increases in lift are observed close to the static stall angle at $\alpha = 20°$, where ΔC_L exceeds 0.6 (or 100%) and these data are consistent with prior airfoil investigations. There does not appear to be a significant dependence on reduced frequency and this is broadly consistent with trailing-edge pressure changes and lower surface lift contributions observed on the airfoil. This indicates that these metrics are probably the most reliable for assessing changes in airfoil performance when leading-edge pressure ports are not accounted for. There also may be an averaging effect as the reduced frequency varies across the span. Notwithstanding, this near independence on F^+ bodes well for applications in which it is difficult to accurately determine the crosswind speed. Indeed, even an error on the order of 100% will still produce a substantial, although not necessarily optimum, result.

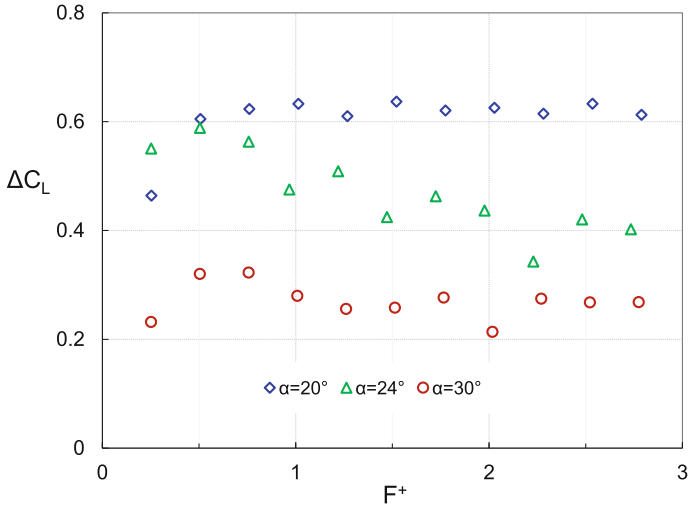

Fig. 8 Post stall panel lift dependence on reduced frequency scan at $U_\infty = 22$ m/s: d.c. = 10%, $\Pi_{\text{gross}} = 8.7$ W

Baseline and controlled tuft flow visualization at $\alpha = 20°$, under conditions corresponding to Fig. 8 ($F^+ = 0.75$ d.c. = 10%), are shown in Fig. 9. Baseline orientation of the tufts, also visible in video recordings, show apparently random motion. When actuation is applied, the flow appears to attach fully both near the root and tip. However, slightly inboard from the tip and close to the trailing-edge, there exists a flow component towards the root that increases further inboard. At approximately the mid-span position the leading-edge flow has a tip-wise component and the result is a vortical flow with its axis approximately normal to the panel surface. Close inboard, the flow has a component towards the root near the trailing-edge. However, further outboard a similar but opposite-signed vortical structure is evident on the surface and the net result appears to be a stall-cell. However, video recordings show that this structure is not stationary and tends to meander inboard in a wave-like manner along the span.

An example of the lift coefficient versus angle of attack is shown in Fig. 10 for baseline and actuation cases at $U_\infty = 22$ m/s. In addition to significant post-stall lift increases, actuation is also clearly capable of almost eliminating hysteresis associated with the panel. However, actuation is not capable of materially increasing $\Delta C_{L,\max}$, due to the fact that the actuator thrust (or body force) is too low. To increase $\Delta C_{L,\max}$ by approximately 0.1, significantly greater plasma thrust, typically an order of magnitude increase, will be required. On the basis of other investgations, this certainly appears to be attainable [19].

When a V-tail configuration is subjected to a crosswind, the panels experience different conditions depending upon whether they are on the windward or leeward side of the vehicle. On the windward and leeward sides, the angle-of-attack will

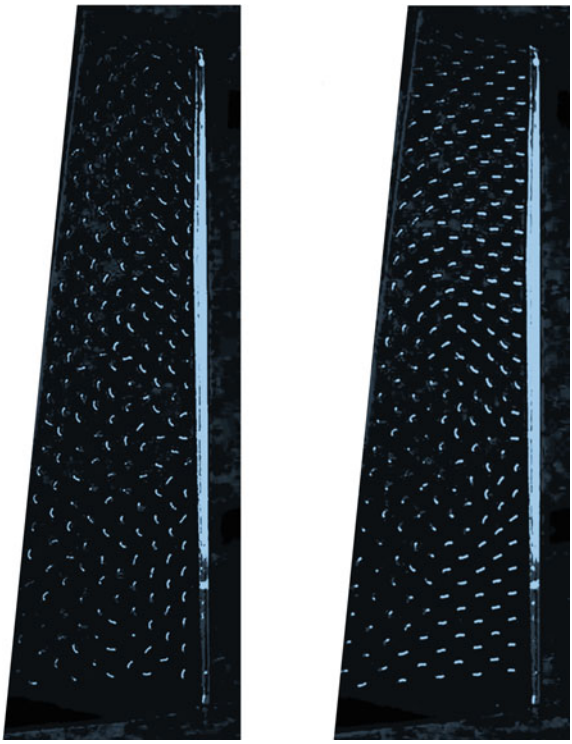

Fig. 9 Panel flow visualization at $U_\infty = 22$ m/s and $\alpha = 20^{\circ}$: left baseline; right $F^+ = 0.75$, d.c. = 10%

increase and decrease respectively. Furthermore, the crosswind also produces an effective sweep-back or sweep-forward depending on whether the panel is leeward or windward respectively. It is important to note that sweep has a non-negligible effect on the mechanism and effectiveness of leading-edge separation control [20] and will be considered in the next phase of this research effort.

To illustrate the effect of plasma-based flow control on takeoff performance, estimates were made by accounting for the effect of sweep [20]. Well-known vehicle performance stability and control software [21] was employed, subject to the assumptions that rotation occurs at 1.15 V_{stall} and downwash in ground effect is accounted for. Based on the experimental data, it was seen that plasma actuation increased the allowable crossflow wind speed from 7.7 m/s (15 kts) to 12.9 m/s (25 kts). This is a meaningful result because, in many locations, wind speeds in excess of 12 m/s are highly improbable.

Furthermore, to better understand the practical weight and power requirements for flight applications, consider, for example, a stack of three typical 12 Volt LiPo batteries (dimensions: 25 × 34 × 104 mm; mass: 183 grams; and capacity 2.2 Ah). These specifications should be compared to the vehicle gross weight (450 kg), payload (150 kg) and endurance (20–30 h). The three batteries add less than 600 g, negligible volume and can operate continuously on two panels for approximately nine hours.

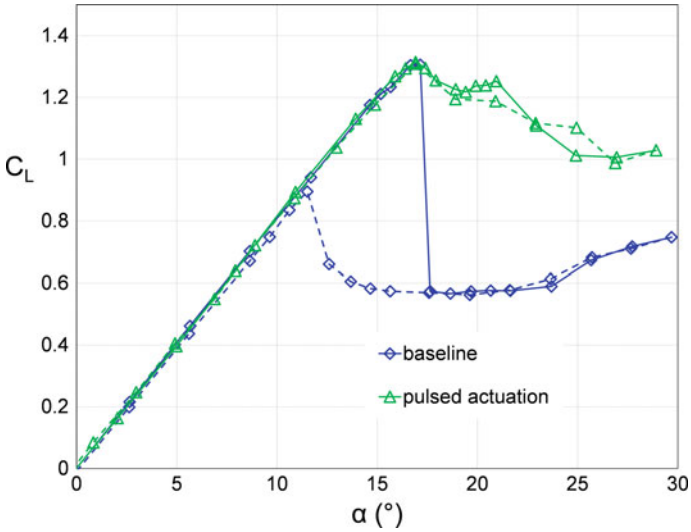

Fig. 10 Full-scale panel lift coefficient as a function of angle of attack at $U_\infty = 22$ m/s. Actuation parameters: $F^+ = 0.75$, $f_p = 36$ Hz, d.c. = 10%, $f_{\text{ion}} = 5500$ Hz, $\Pi_{\text{gross}} = 8.7$ W/m, $V_{\text{pp}} = 16.1$ kV. Solid line—increasing α; dashed line—decreasing α

Clearly, these numbers can be improved upon, but they illustrate that the weight, volume and power requirements of the plasma actuation system are well within achievable bounds.

4 Concluding Remarks

The major conclusion of this study is that pulsed DBD plasma actuators are a viable and practical solution to the problem of separation control on V-tail panels, resulting from crosswinds during takeoff and landing. In terms of performance, post-stall lift coefficient increases of 0.6 (or 100%) were observed and bi-stable behavior (hysteresis) was eliminated even under deep stall ($\alpha = 30^{\text{o}}$) conditions. Low power requirements (<10 W) can easily be fulfilled off-line, using batteries (<1 kg); the high-voltage generators are a small fraction of the payload (typically 1.0 kg); the actuator themselves are lightweight (around 100–300 g). The relative insensitivity to reduced frequency in the range examined here, between 0.5 and 2.5, also renders the system very robust. Throughout all experiments, no burn-through and no failures whatsoever were encountered and no oxidation or degradation of the silicone rubber dielectric was observed after completion of the experiments.

Future investigations should integrate the actuator into the geometry of the tail element. Thus the only disturbance on the element will be a <25 μm external electrode. Removal of this electrode with an integrated dielectric results in the original clean

element configuration. The external electrode is easy to replace or remove. Total failure of the DBD plasma system causes the vehicle to perform in its baseline configuration. Prior to flight testing, greater body forces must be generated using thicker dielectrics, up to O(10 mm), with a target $C_\mu = O(0.1)\%$. This will not materially increase input power, but will require significantly higher V_{rms}. Finally, conditions of forward- and backward-sweep must be fully evaluated prior to flight-testing and actuation must be achievable on both sides of the panel.

Acknowledgements This research was supported, in part, by the Nancy and Stephen Grand Technion Energy Program (GTEP). The authors also wish to thank the staff of Israel Aircraft Industry's (IAI's) Low Speed Wind Tunnel for assistance in performing the full-scale panel experiments.

References

1. Purser, P.E., Campbell, J.P.: Experimental Verification of a Simplified Vee-Tail Theory and Analysis of Available Data on Complete Models with Vee-Tails, NACA Rept. 823 (1945)
2. Abzug, M.J.: V-Tail stalling at combined angles of attack and sideslip. AIAA J. Aircr. **36**(4), 729–731(1999). https://doi.org/10.2514/2.2500
3. Corke, T.C., Post, M.L., Orlov, D.M.: SDBD plasma enhanced aerodynamics: concepts, optimization and applications. Prog. Aerosp. Sci. **43**, 193–217 (2007)
4. He, C., Corke, T.C., Patel, M.P.: Plasma flaps and slats: an application of weakly ionized plasma actuators. AIAA J. Aircr. **46**(3), 864–873 (2009)
5. Sosa, R., Artana, G., Moreau, E., Touchard, G.: Stall control at high angle of attack with plasma sheet actuators. Exp. Fluids **42**, 143–167 (2007). https://doi.org/10.1007/s00348-006-0227-5
6. Kelley, C.L., Bowles, P., Cooney, J., He, C., Corke, T.C.: High mach number leading-edge flow separation control using AC DBD plasma actuators. In: 50th AIAA Aerospace Sciences Meeting Including the New Horizons Forum and Aerospace Exposition, 9–12 January 2012, Nashville, Tennessee. AIAA Paper No. 2012-0906 (2012)
7. Roupassov, D.V., Nikipelov, A.A., Nudnova, M.M., Starikovskii, AYu.: Flow separation control by plasma actuator with nanosecond pulsed-periodic discharge. AIAA J. **47**(1), 169–185 (2009)
8. Little, J., Takashima, K., Nishihara, M., Adamovich, I., Samimy, M.: High lift airfoil leading edge separation control with nanosecond pulse driven DBD plasma actuators. In: 5th AIAA Flow Control Conference, 28 June–1 July 2010, Chicago, Illinois. AIAA Paper No. 2010-4256 (2010)
9. Greenblatt, D., Göksel, B., Rechenberg, I., Schule, C., Romann, D., Paschereit, C.O.: Dielectric barrier discharge flow control at very low flight Reynolds numbers. AIAA J. **46**(6), 1528–1541 (2008)
10. Greenblatt, D., Schneider, T., Schule, C.Y.: Mechanism of flow separation control using Plasma Actuation. Phys. Fluids **24**, 077102 (2012). https://doi.org/10.1063/1.4733399
11. Göksel, B., Greenblatt, D., Rechenberg, I., Nayeri, C.N., Paschereit, C.O.: Steady and unsteady plasma wall jets for separation and circulation control. In: 3rd AIAA Flow Control Conference, 5–8 June 2006, San Francisco. California, USA. AIAA Paper 2006-3686 (2006)
12. Greenblatt, D., Schulman, M., Ben-Harav, A.: Vertical axis wind turbine performance enhancement using plasma actuators. Renew. Energy **37**, 345–354 (2012). https://doi.org/10.1016/j.renene.2011.06.040
13. Ben-Harav, A., Greenblatt, D.: Feed-forward dynamic stall control on a vertical axis wind turbine. Wind Energy **19**(1), 3–16 (2016). https://doi.org/10.1002/we.1814
14. Greenblatt, D., Ben-Harav, A., Mueller-Vahl, H.: Dynamic stall control on a vertical-axis wind turbine using plasma actuators. AIAA J. **52**(2), 456–462 (2014). https://doi.org/10.2514/1.J052776

15. Greenblatt, D., Lautman, R.: Inboard/outboard plasma actuation on a vertical-axis wind turbine. Renew. Energy **83**, 1147–1156 (2015)
16. Greenblatt, D., Wygnanski, I.: The control of separation by periodic excitation. Prog. Aerosp. Sci. **36**(7), 487–545 (2000)
17. Duchmann, A., Simon, B., Tropea, C., Grundmann, S.: Dielectric barrier discharge plasma actuators for in-flight transition delay. AIAA J. (in press). https://doi.org/10.2514/1.J052485
18. Greenblatt, D.: Unsteady low-speed wind tunnels. AIAA J. **54**(6), 1817–1830 (2016)
19. Thomas, F.O., Corke, T.C., Iqbal, M., Kozlov, A., Schatzman, D.: Optimization of dielectric barrier discharge plasma actuators for active aerodynamic flow control. AIAA J. **47**(9), 2169–2178 (2009)
20. Greenblatt, D., Washburn, A.E.: Influence of finite span and sweep on active flow control efficacy. AIAA J. **46**(7), 1675–1694 (2008)
21. Williams, J.E., Vukelich, S.R.: The USAF Stability and Control Digital DATCOM, vol. I. Users Manual (1979). ADA086557, www.dtic.mil/dtic/tr/fulltext/u2/a086557.pdf